Journal of Marine Systems 78 (2009) S181–S190

Contents lists available at ScienceDirect

Journal of Marine Systems

journal homepage: www.elsevier.com/locate/jmarsys

Mixed layer depth in the Aegean, Marmara, Black and Azov Seas: Part II: Relation to the sonic layer depth

Robert W. Helber [a,*], A. Birol Kara [a,1], Charlie N. Barron [a,2], Timothy P. Boyer [b,3]

[a] Ocean Dynamics and Prediction, Naval Research Laboratory, Stennis Space Center, MS 39529-5004, United States
[b] NOAA/NODC,SSMC III, E/OC5, 1315 East West Highway, Silver Spring, Maryland 20910, United States

ARTICLE INFO

Article history:
Received 18 December 2007
Received in revised form 21 August 2008
Accepted 22 January 2009
Available online 3 March 2009

Regional index terms:
The Aegean Sea
The Black Sea
The Azov Sea

Keywords:
Sound transmission
Mixed layer depth
Climatology

ABSTRACT

This paper provides the first analysis of the seasonal evolution of the sonic layer depth (SLD) relative to the mixed layer depth (MLD) for the Aegean, Marmara, Black, and Azov Seas. SLD identifies the acoustic ducting capabilities of the upper ocean and is of interest to investigations of upper ocean acoustics. A monthly SLD climatology on a regular $0.25^\circ \times 0.25^\circ$ grid is constructed from interpolation of available quality-controlled ocean temperature and salinity profiles using the kriging methodology. A four step pre-processing procedure is designed to reduce noise and the effects of sampling irregularities. Monthly SLD fields are then compared relative to the much more widely studied MLD as computed using four different methods from the recent scientific literature. The goals of this analysis are to characterize the SLD relative to the MLD and provide a means for computing SLD from limited hydrographic information and/or MLD estimates. Very deep SLD values are found during winter, in the Aegean and Black Seas, when the near surface temperature values become lower than the temperature below the permanent pycnocline. When this occurs, the SLD drops to the bottom while the MLD remains much shallower at the seasonal pycnocline. For the months of May through October the SLD tends to be less than 25 m for the entire region. It is demonstrated that MLD obtained from the four methodologies have high correlations with SLD over the annual cycle, indicating a robust relationship. As a result, SLD can be estimated using least squares regression coefficients when salinity is unavailable or when observation profiles do not extend to deeper levels.

Published by Elsevier B.V.

1. Introduction

Conditions of the upper ocean often result in a near surface acoustic duct that limits the downward transmission of sound and results in the acoustic spreading to be approximately cylindrical (Urick, 1983). Sound trapped in a surface duct is primarily transmitted outward from the source in an expanding disk. This occurs when the near surface environment is upward refracting due to an increase of sound speed with depth. The depth over which the increasing sound speed penetrates is called the sonic layer depth (SLD) (e.g., Kerman, 1993). The acoustic frequency that can propagate in this type of duct is dependent on the SLD. For a given SLD there is a cutoff frequency above which sound will be trapped in the surface duct. Sound with a lower frequency is not trapped and will spread spherically in all directions, leading to more rapid horizontal attenuation (Etter, 2003). Sound in a duct (with cylindrical spreading) can be transmitted much farther horizontally than in non-ducting environments (with spherical spreading). This phenomenon substantially influences, for example, ocean communications (Siderius et al., 2007), acoustic tomography (Sutton et al., 1993), and naval operations (Urick, 1983).

A parameter related to SLD, the mixed layer depth (MLD), is also important because it identifies the penetration depth of turbulence near the ocean surface and has a wide array of influence on a variety of upper ocean processes from air-sea exchange (e.g., Chen et al., 1994) to biological interactions (e.g., Siegel et al., 2002). For a typical water column, where isothermal and isohaline surface layer depths are equal and temperature decreases below that depth, the MLD and SLD are equal. This is because sound speed increases with depth due only to increasing pressure until a local maximum at the MLD, below which sound speed decreases with decreasing temperature. There are other conditions, however, where the SLD may be lower or higher in the water column than the MLD. The characteristics of how SLD and MLD become different are discussed in this paper because they provide useful information regarding the structure of the upper ocean temperature and salinity fields.

In a recent analysis (Helber et al., 2008), the global deviations of the MLD relative to the SLD were investigated for the annual cycle. It was

* Corresponding author. Tel.: +1 228 688 5430; fax: +1 228 688 4759.
E-mail addresses: robert.helber@nrlssc.navy.mil (R.W. Helber), birol.kara@nrlssc.navy.mil (A.B. Kara), charlie.barron@nrlssc.navy.mil (C.N. Barron), boyer@nodc.noaa.gov (T.P. Boyer).
URL: http://www.7320.nrlssc.navy.mil (R.W. Helber).
[1] Tel.: +1 228 688 4537.
[2] Tel.: +1 228 688 5423.
[3] Tel.: +1 301 713 3290x186.

0924-7963/$ – see front matter. Published by Elsevier B.V.
doi:10.1016/j.jmarsys.2009.01.023

found that in the spring when new stratification events occur, the SLD can be substantially deeper than the MLD. In the present study, we examine differences between SLD and MLD in more detail in a region including a small part of the eastern Mediterranean Sea and the Aegean, Marmara, Black and Azov Seas. This is accomplished by interpolating the SLD and MLD values to a 0.25×0.25 grid using kriging (Diggle and Ribeiro, 2007). This region is chosen because there have not been any previous studies quantifying and examining SLD features.

The Black Sea is heavily influenced by river input that along with precipitation exceeds evaporation losses and is balanced by outflow across the Bosphorus (Özsoy and Ünlüata, 1998). As a result, the Black Sea is characterized by fresher surface water residing above warmer saltier deep water (a condition associated with "diffusive convection," e.g., Kantha and Clayson, 2000). Above a permanent pycnocline there exists a cold intermediate layer (CIL) that is replenished in the winter when the seasonal thermocline is deepest (Özsoy and Ünlüata, 1998). The Aegean Sea is influenced by cooler fresher surface water originating in the Black Sea that passes through the Bosphorus and the Marmara Sea and enters the Aegean through the Dardanelles Strait. This water flows across the northern Aegean shelf and southward along the western coastline (Kourafalou and Barbopoulos, 2003; Olson et al., 2007). Cold, saltier Mediterranean water enters the lower layers of the Marmara Sea through the Dardanelles Strait (Beşiktepe et al., 1994). The Sea of Azov is very shallow, with an average depth of 5 m, but stratification does exist (Debolskaya et al., 2008). In all of these regions, to some degree, the surface layers defined by MLD and SLD will be associated with cooler, fresher surface water above saltier, warmer subsurface water. As will be shown, the evaluation of the SLD relative to the MLD is impacted by this unique hydrographic structure, making this an excellent region for studying SLD and its relation to MLD.

Estimating SLD from observation profiles is achieved using a method derived by Helber et al. (2008). We use four methodologies for MLD taken from the recent literature (Kara et al., 2000b; Lorbacher et al., 2006) that are discussed by Kara et al. (2009). For two of the algorithms, temperature-only profiles are used, while the other two select the MLD from density profiles. Comparison of SLD with both temperature and density MLD estimates, all interpolated on a 0.25° grid, provide information regarding the salinity contribution to the upper ocean in addition to characterizing upper ocean acoustics and the penetration depth of surface turbulence. Use of several MLD methods enhances the results by ensuring that the observed phenomena are not an artifact of one MLD methodology.

The differences between the SLD and MLD arise because of differences in the sensitivities of density and sound speed to temperature, salinity, and pressure. For density, salinity variability is often small enough that the MLD is controlled by temperature. Salinity, however, can have a large impact producing, for example, the "barrier layer" (e.g. Kara et al., 2000a), where the salinity contribution results in a MLD that is shallower than temperature alone would dictate. Salinity has a smaller impact on sound speed relative to density because sound speed is more sensitive to temperature than salinity. A fundamental difference between sound speed and density, and therefore SLD and MLD, is that sound speed does not influence turbulence whereas density does. These differences results in a relationship between SLD and MLD that we explore in this analysis.

A major goal of this paper is to identify the conditions under which SLD and MLD differ in time and space in the Aegean, Marmara, Black and Azov Seas region. In addition, statistical relationship between SLD and MLD is exploited in order to provide a means for predicting SLD from MLD estimates. This capability is particularly useful when only temperature profiles or MLD forecasts are available.

In Section 2 we describe the sources of the observation profiles and the quality control and data editing procedures. The methods for estimating MLD, SLD and computing the interpolated fields are described in Section 3. The monthly SLD climatology is described in Section 4 and the differences between SLD and MLD are discussed in Section 5. Section 6 describes the statistical relationship of SLD and MLD and Section 7 concludes the paper. The Appendix A contains information about the data preparation steps taken for producing the interpolated SLD/MLD 0.25° gridded fields.

2. Data

The available historically observed temperature profiles (T-only) and paired profiles of temperature and salinity (T and S) are acquired from the following sources: (1) the World Ocean Database 2005 (WOD05) (Boyer et al., 2006), (2) the U. S. Navy's Master Oceanographic Observation Data Set (MOODS) (Teague et al., 1990), (3) Argo (Gould et al., 2004), and (4) the National Oceanographic Data Center (for the Sea of Azov, Matishov et al., 2006). The reader is referred to Table 1 for the number of profiles of T-only and T and S from each source. The first three sources of data are partially redundant but all are considered, because after the removal of duplicates there are unique data in each. The WOD05 has less stringent quality control (QC) procedures than MOODS but potentially more data sources. There is an approximately 6% increase in data volume with the addition of WOD05 data relative to the MOODS data set alone. Older Argo data are included in the MOODS and WOD05, and the latest Argo data from the Data Acquisition Centers (DAC) have been included with the application of the latest QC recommendations. As an example of the data coverage for observations with profile pairs of T and S, Fig. 1 shows the locations of usable profiles for all years in the month of October only. Note that for the Marmara and Azov Seas there are very few data points, and therefore the results within these seas is less robust than in the Black and Aegean Seas.

While the data are quality-controlled, there are still some existing errors that include profile location, XBT drop rate, low vertical resolution, etc. In the interest of including as much data as possible, profiles with relatively low vertical resolution or large gaps in the vertical have been retained in the data set. To help minimize these and other sources of potential errors, SLD "outliers" are removed statistically as explained in Appendix A. Errors that are not also "outliers" are statistically undetectable and therefore cannot be removed in this manner.

3. Methods

The SLD algorithm is described in detail in Helber et al. (2008) and will be explained briefly here. The first step in estimating the SLD from T and S profile pairs is the computation of sound speed at each depth level using the nine-term equation of Mackenzie (1981):

$$c = 1448.96 + 4.591T - 5.304 \times 10^{-2}T^2 + 2.374 \times 10^{-4}T^3 + 1.340(S-35) + 1.630 \times 10^{-2}D + 1.675 \times 10^{-7}D^2 - 1.025 \times 10^{-2}T(S-35) - 7.139 \times 10^{-13}TD^3$$

Sound speed, c (m s^{-1}), is a function of temperature, T (°C), salinity, S (psu), and depth, D (m) and is non-linear. The first three non-constant terms depend only on T and are the largest in the upper ocean. Only at depth do the terms including D have large

Table 1
The number of total, T-only, and T and S profiles from each source in the analysis domain of Fig. 1 (22.00 E to 41.84 E and 34.50310 N to 47.31377 N).

Source	Total	T-only	T and S
All	105,164	70,516	34,648
Argo	3010	3	3007
WOD05	64,031	53,560	10,471
MOODS	37,659	16,935	20,724
NODC (Azov)	464	18	446

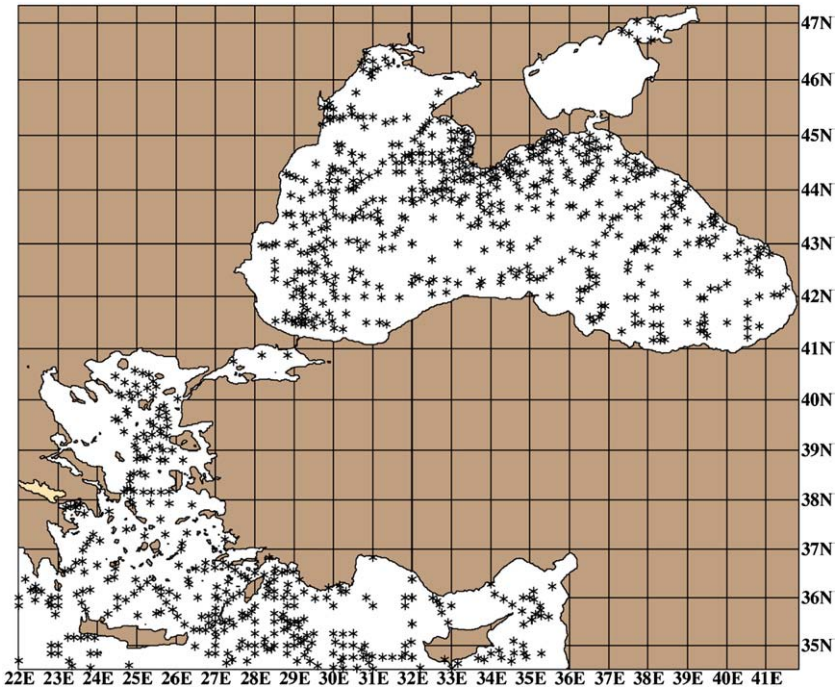

Fig. 1. Observation locations for *T* and *S* profiles with at least three usable depth levels over the study region in the month of October. Profiles with *T*-only are more numerous and are not shown.

contributions. As noted earlier, sound speed is less sensitive to *S* than to *T*, as compared to density for typical oceanic values for *T* and *S*.

Starting at the surface downward, each depth level ($k = 1,2,3,\cdots K$) of a given profile is examined using two criteria:

(1) Is the *k*th sound speed value greater than those at levels less than *k*
(2) Is the *k*th sound speed value greater than that at level $k+1$

Each depth level that satisfies the above 2 criteria identities a local depth maximum in sound speed and an overall upward refracting (negative) sound speed gradient from the surface to the *k*th depth level. If more than one data level meets these criteria, several other tests are conducted to identify the nature of the sound speed gradient above each level. In most cases the deepest identified level that meets the criteria is taken as the SLD, but there are additional tests conducted to eliminate potential SLD errors that arise with these simple criteria and to omit solutions that are inappropriate for a particular application.

The tests are employed using two tuning parameters that represent the average frequency (on a log scale) and the lowest frequency expected for an acoustic application. For this study we chose a low frequency range generally used in Navy operations (Kunz and Gauss, 2000) defined by the mid and lowest frequencies of 680 Hz and 70 Hz, respectively. For example, a test is conducted to check for the existence of a subsurface duct above each of the identified data levels. In cases where there is a subsurface duct, the SLD is non-existent and is set to zero. To determine the presence of a subsurface duct, the minimum cutoff frequency is computed by integrating the sound speed profile (Etter, 2003). If the frequency is greater than the mid frequency (680 Hz) then the duct above the identified level is large enough to negate the existence of a surface duct and SLD is set to zero. Additional tests, to ensure the proper SLD is identified, are described by Helber et al. (2008).

Four different MLD methodologies are employed to help identify only the most robust relationships between SLD and MLD. We have chosen two algorithms that are based solely on *T*-only profiles and two algorithms that require *T* and *S* profiles. As described by Kara et al. (2009) the T-only methods are an isothermal threshold method (Kara et al., 2000b) denoted MLD(T) and a curvature based method (Lorbacher et al., 2006) denoted MLD(L). The methods that require both *T* and *S* to compute σ_t are a variable σ_t threshold method (Kara et al., 2000b) denoted MLD(σ_T) and a constant density threshold method denoted MLD(σ_C) employed using the programs of Kara et al. (2000b). Hereafter, MLD will be used to represent the mixed layer depth in general, while the notation MLD(L), MLD(T), MLD(σ_T), and MLD(σ_C) will represent the MLD as estimated from observations using the associated methodologies listed above.

To create monthly gridded fields of SLD and MLD we have processed the data to reduce noise and normalized the error levels using several steps described in the Appendix A. These climatologically processed observations represent an unknown underlying process and contain unavoidable noise. The noise comes from, for example, interannual variability, systematic and random errors, and inhomogeneous sampling. With this in mind, interpolation of the irregular data locations are then performed using kriging. Kriging takes into account the presence of noise and constructs a linear predictor based on the covariance structure of the data (Cressie, 1991; Diggle and Ribeiro, 2007). The kriging parameters that control the linear predictor and the amount of smoothing applied to the output field are the range ϕ, sill σ'^2, and nugget. Using an empirical technique, the sill and nugget are linearly fit to the biweight standard deviation of the data using a range of 2.5°. The nugget is chosen such that the amount of smoothing applied has a characteristic length equal to 1.4°. The details of this procedure are described in Kara et al. (2009).

4. Monthly SLD climatology

Following methods in the Appendix A and the kriging interpolation described in the Section 3 and in Kara et al. (2009), we now present the monthly mean SLD fields and compare them to the four MLD fields mentioned above. It can be seen in Fig. 2 that the SLD has a seasonal cycle with relatively deep SLD during months of January, February, and March. February has the greatest extent of very deep SLDs. In the southern part of the Aegean Sea and the south western part of the Black Sea the SLD is deeper than 200 m during January and February. During March the deep SLDs are restricted to the center of the western Black Sea gyre and isolated regions of the Aegean Sea. Because of the deep

SLD values, January, February, and March would be good months for long range upper ocean acoustic communication.

The very deep SLD values occur at these locations during winter when the surface temperatures are cooler than the deep water temperatures. There is a permanent pycnocline at 50–100 m in the Black Sea that occurs at the bottom of the CIL (Özsoy and Ünlüata, 1998) and below 500 m the water of Mediterranean origin is essentially well-mixed (Poulain et al., 2005). When the near surface temperatures are below approximately 8 °C (or the temperature of the CIL), the sound speed increases with depth all the way to the bottom and consequently the SLD is also at the bottom (Fig. 2). An example profile is shown in Fig. 3.

This phenomenon has sharp transitions in space and time. As near surface temperatures seasonally become cooler in the fall, the SLD becomes gradually deeper until the surface temperatures dip below the temperatures of the CIL. At this point the SLD immediately drops to the bottom. This shift to deep SLDs occurs in short distances horizontally as can be seen in Fig. 2 for months of January, February, and March where large SLD gradients occur around the deep SLD (red) areas. The standard deviation of SLD is also large during the months where deep SLDs occur (Table 2).

For these deep SLD cases there is some ambiguity. Many CTD casts do not go to the bottom. For a sound speed profile that is upward refracting over the whole water column, the actual SLD would be at the ocean bottom but the analysis of the observation would put the SLD at the bottom of the CTD cast. For this reason, Fig. 2 does not show the SLD variability when the SLD is deeper than 200 m.

The seasonal cycle of SLD can also be seen in the time series at various point locations (Fig. 4). The deepest SLDs and the largest seasonal variability occur in the western gyre of the Black Sea in February (see also Table 2). The smallest variability is during the months of May through September and in the relatively shallow Sea of Azov (Fig. 2). The Aegean Sea has a longer deep SLD season that starts sooner and ends later than in the Black Sea.

5. Differences between SLD and MLD

Comparisons between different types of surface layers provide information regarding the upper ocean structure. For example, when the SLD is deeper than the MLD, salinity and temperature both tend to increase with depth (Fig. 3). Salinity must increase with depth at a sufficient rate, because otherwise the profile would be unstable. When

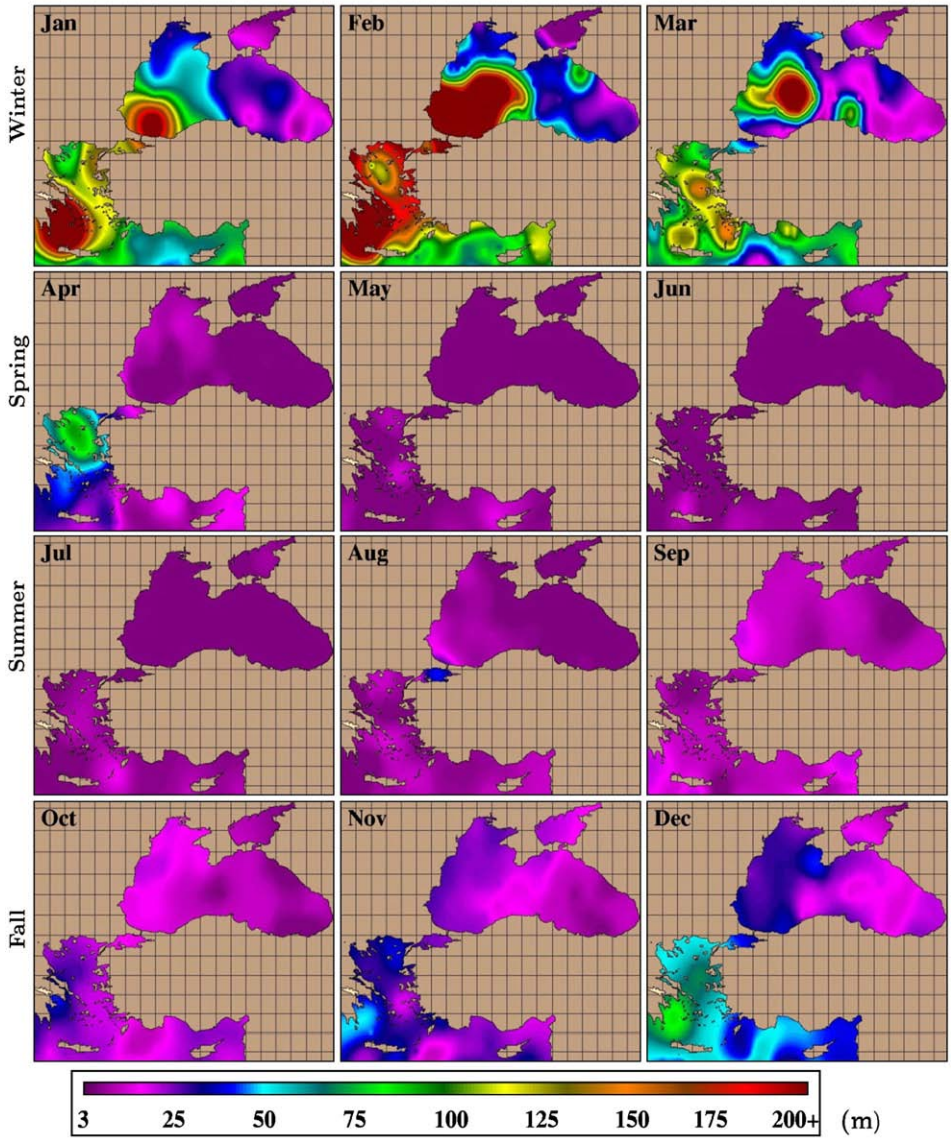

Fig. 2. Monthly mean SLD climatology in the Aegean, Marmara, Black and Azov Seas by month. SLD fields are produced based on individual *T* and *S* profiles available from WOD05, MOODS, and Argo data archives. See text for further details. The color palette is the same for all months to show seasonal variability.

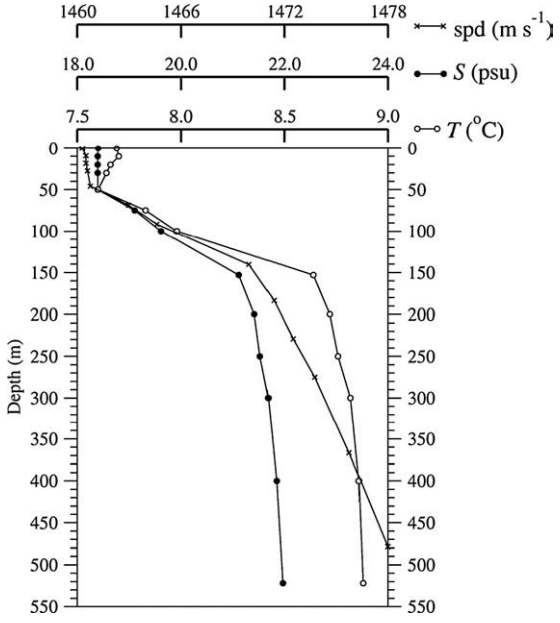

Fig. 3. An example profile where the SLD exists at the bottom of the profile, SLD = 522 m. The location of the profile is 30°N, 43°E taken on 19/02/1975 and MLD(T) = 141, MLD(σ_T) = 53, MLD(σ_C) = 55, and MLD(L) = 10 m.

the MLD is deeper than the SLD, it is because SLD responds to small sound speed maxima in profiles that are relatively uniform with depth (Fig. 6). To explore these relationships further, we investigate whether or not SLD is typically deeper than, shallower than, or identical to MLD.

Monthly mean MLD climatologies based on the four MLD methodologies discussed in Section 3 are used to compute differences between SLD and MLD. As evident from Fig. 5, SLD can be deeper or shallower than MLD depending on the month of the year. This is true regardless of which method is used for computing MLD. There are two main features in the SLD versus MLD differences. The SLD is typically much deeper than MLD in the southwestern Black Sea and parts of the Aegean Sea in January (Fig. 5a) and February and March (not shown). When SLD drops to the bottom, as described in Section 4, the MLD remains with the seasonal pycnocline. During February the difference is so large and widespread that it even dominates the basin-wide average (Table 3). This difference is enhanced for the MLD(L) field due to its wintertime shallow bias (Kara et al., 2009). The difference in SLD-MLD(L) is on average 77 m over the study region (Table 3). The variance of the basin-wide difference fields is considerably larger during winter and early spring due to the variance in SLD (Table 3).

The other main feature is that MLD is deeper than SLD over the entire Black Sea for the rest of the year, but the magnitude of this bias is generally smaller. The values for the difference SLD-MLD in Table 3 are mostly negative for all months except February. The MLD(L) results are the exception. An area where MLD can be considerably deeper than SLD is in the spring when new stratification occurs in the Aegean Sea (Fig. 5b). This bias is absent for MLD(L) because the curvature based methodology detects small temperature deviations associated with new stratification (Helber et al., 2008). These small

Table 2
Monthly standard deviation of the SLD for the Black Sea between latitudes 41°N and 45°N.

Month	Jan	Feb	Mar	Apr	May	Jun	Jul	Aug	Sep	Oct	Nov	Dec
SLD standard deviation, m	38	212	128	23	7	4	6	9	13	16	23	29

Outlier removal using the Z-score statistic (see Appendix A) was applied prior to the computation of the standard deviation.

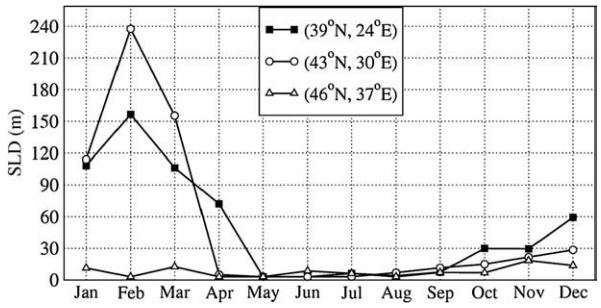

Fig. 4. Climatological mean time series of SLD at three locations over the annual cycle. These locations are randomly chosen to represent typical SLD values in the Aegean (39°N 24°E), Black (43°N 30°E) and Azov Seas (46°N 37°E).

deviations are also sufficient to create a SLD at that depth (Fig. 6). Since the variance of temperature with depth is relatively small, the MLD(σ_T) and MLD(σ_C) values remain deeper. The MLD(L) values generally remain closer to SLD than the MLD(σ_T) and MLD(σ_C) values except for during the deep winter SLD regions. During the boreal summer and fall, SLD remains shallower than all four MLDs (Fig. 5c,d).

To illustrate the differences between SLD and MLD(σ_T) in another way, we produce a scatter diagram in January (Fig. 7) and July (Fig. 8). The kriging interpolation field data are used to construct the figures. For January there exists a statistically significant linear correlation coefficient of 0.74. There are two off diagonal "lobes:" (1) in the left side of Fig. 7 where MLD(σ_T) is between 50 and 100 m that represents values primarily in the Black Sea (Fig. 5) and (2) the lower right side of Fig. 7 where SLD is between 50 and 125 m that represents values in the Mediterranean.

For July there is no statistically significant linear correlation, because there are two competing regions with different characteristics. One region is where SLD is essentially zero and the other is where SLD is non-zero but smaller than MLD(σ_T). When SLD is not zero, it is still shallower than MLD(σ_T). Regionally, correlation between SLD and MLD is significantly higher, as will be shown in Section 6. This is evident in the scatter plots of Figs. 7 and 8 because each of the "lobes" represents a region of high correlation.

6. Relationship between SLD and MLD

In this section we seek a simple relationship between SLD and MLD values over the seasonal cycle. This could help identify regions where SLD can be obtained from T-only profiles using MLD(L) or MLD(T) and a simple computation, e.g., adding or subtracting a constant offset. This could be advantageous over the alternative of using T and S profiles, which are generally less available than T-only profiles. In addition, for T-only observations that extend less than 200 m, as for many bathythermographs, such a relationship could be used to estimate the SLD that could be much deeper. We use all MLD climatologies in seeking a relationship to test the sensitivity of the statistics to the MLD definition.

We evaluate time series of SLD and MLD over the seasonal cycle. The statistical relationships used in comparisons between the 12 monthly MLD (X) and SLD (Y) values at each grid point are expressed as follows:

$$R = \frac{1}{n}\sum_{i=1}^{n} (X_i - \overline{X})(Y_i - \overline{Y}) / (\sigma_X \sigma_Y), \quad (1)$$

where

$$Y = a + bX + c \quad (2)$$

and $n = 12$, R is the correlation coefficient, and $\bar{X}$ ($\bar{Y}$) and σ_X (σ_Y) are the mean and standard deviations of MLD (SLD) values, respectively.

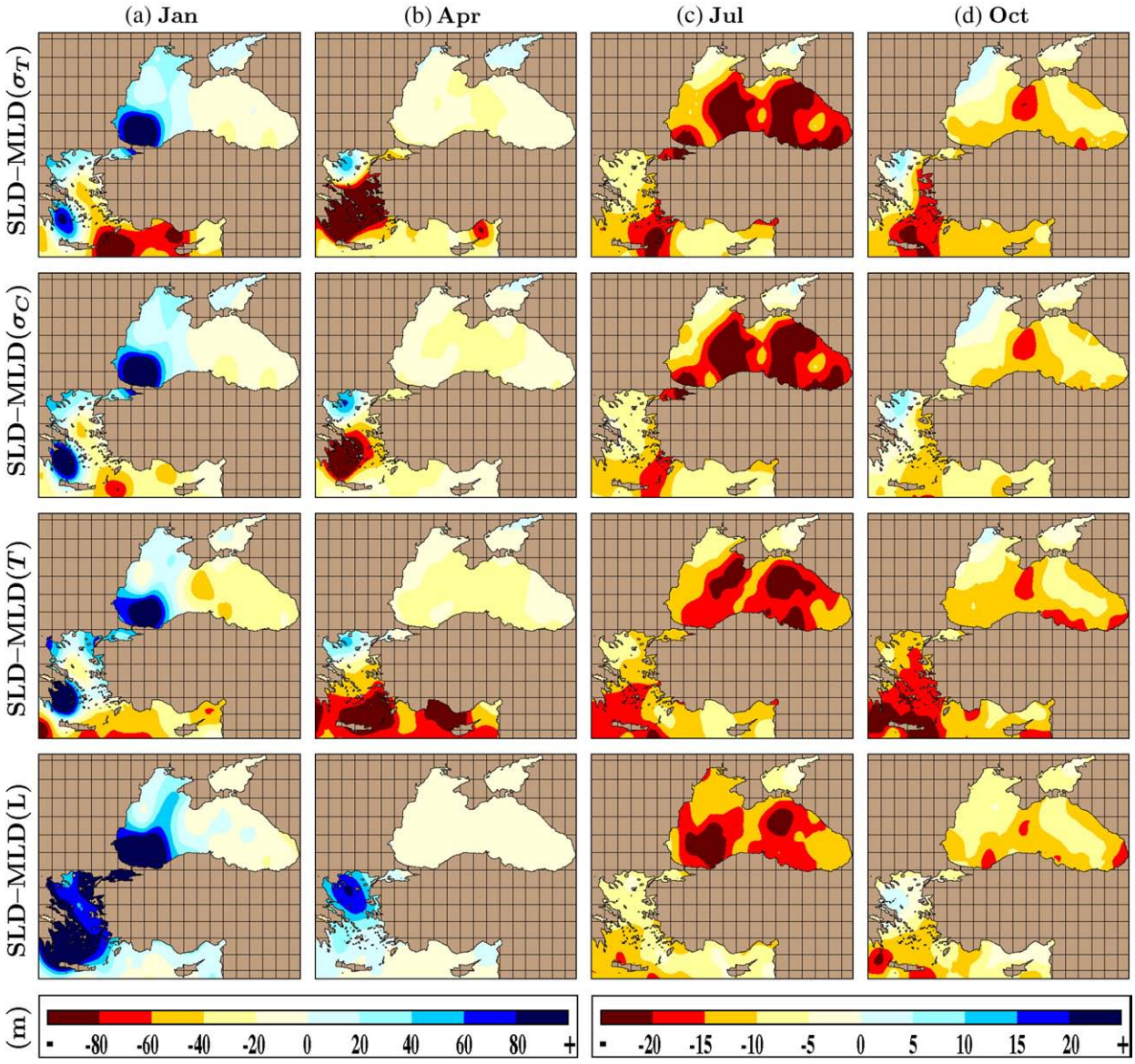

Fig. 5. Differences between SLD and the four MLD definitions MLD(σ_T), MLD(σ_C), MLD(T), and MLD(L). Results are shown in (a) January, (b) April, (c) July and (d) October, separately. Note the color palette for the difference fields in January and April is different from that in July and October.

In the regression Eq. (2), Y is the dependent variable, X is the independent variable (or covariate), a is the intercept, b is the slope or regression coefficient, and c is the error term. The regression equation will specify the average magnitude of the expected change in SLD for the given MLD climatology.

We first determine how SLD and MLD are correlated over the seasonal cycle. The strength of the linear relationship between SLD and MLD is determined by the R value (Eq. (1)), which ranges from −1 to 1. An R value of −1 (1) indicates a very strong, negative (positive) linear relationship, and an R value of 0 indicates no linear

Table 3
SLD differences.

Difference	Jan	Feb	Mar	Apr	May	Jun	Jul	Aug	Sep	Oct	Nov	Dec
SLD-MLD(σ_T)	−8	12	−77	−40	−13	−10	−14	−11	−10	−10	−10	−9
SLD-MLD(σ_C)	2	32	−56	−25	−11	−9	−13	−9	−8	−8	−8	−6
SLD-MLD(T)	−6	18	−61	−39	−15	−11	−14	−12	−13	−12	−15	−16
SLD-MLD(L)	43	77	51	7	−4	−3	−4	−4	−6	−5	−3	4
SD	Jan	Feb	Mar	Apr	May	Jun	Jul	Aug	Sep	Oct	Nov	Dec
SLD-MLD(σ_T)	48	139	145	57	6	4	6	6	4	5	8	13
SLD-MLD(σ_C)	40	114	123	27	4	2	7	6	4	5	6	10
SLD-MLD(T)	45	113	77	33	6	4	5	7	6	5	10	11
SLD-MLD(L)	62	98	47	23	3	3	2	5	4	6	7	14

Basin averaged differences of various mixed layer depths subtracted from SLD.
Standard deviations are calculated from the entire domain (22.00 to 41.84 E, 34.5031 to 47.31377 N) of kriged sea points.

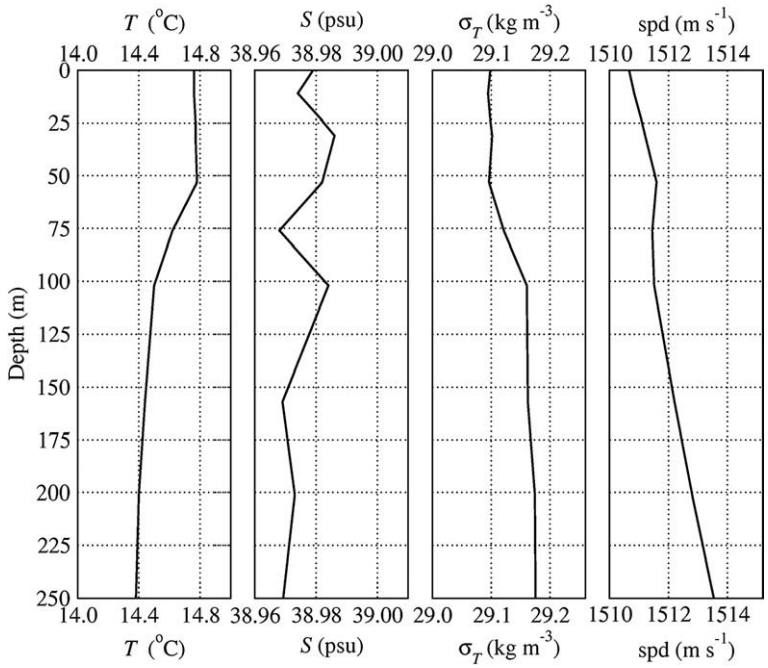

Fig. 6. An example profile during April 1990 where the MLD(L) (53 m) and the SLD (53 m) are relatively shallow while MLD(σ_T) (201 m), MLD(σ_C) (201 m) and MLD(T) (201 m) are considerably deeper.

relationship. The resulting correlations given in Fig. 9 clearly reveal strong and positive values ($R>0.6$) over most of the domain. This is true regardless which MLD methodology is used.

To decide whether or not a correlation value represents a good or poor linear relationship, we apply the student's t-test. Student's t-test is applied to test the null hypothesis that two variables (i.e., SLD and MLD) are not correlated at a given grid point. For the $n=12$ sample values in this paper, the bivariate normal distribution of $t_{n-2} = R\sqrt{n-2}/\sqrt{1-R^2}$ must have an absolute value of at least 0.53 for R to be statistically significant at the 95% ($\alpha=0.05$) confidence level.

Given the significant correlation values over almost the entire domain, including the Aegean, Marmara, Black and Azov Sea, a linear regression can be used to examine the relationship between SLD and MLD. Details of this commonly-used linear regression technique may be found in Wilks (1995). Our objective is to fit a straight line to values between SLD and MLD obtained at each $0.25^\circ \times 0.25^\circ$ over the seasonal cycle. We would like to have a line that is in some sense closest to all of the data points simultaneously, i.e., a method of finding a line via the least squares approach. This process is done at each grid point based on 12-month SLD and MLD time series. Slope and intercept values of the least squares line are then computed as described in Eq. (2).

Fig. 9 shows that slope values are remarkably similar for SLD regressions using any of the MLD methodologies. In particular, slope values are almost constant and negative in the Marmara, Black and Azov Seas. For the western Black Sea the slope is nearly zero while the intercept is positive, indicating that SLD is deeper than MLD and that the difference varies little in magnitude. The Aegean Sea has a different slope for MLD(L) that may be related to its closer relationship with SLD during the spring in that area (Fig. 5b).

There appears to be a salinity contribution to MLD in the Aegean Sea and the northwestern portion of the Mediterranean Sea that is in our study region. For the intercept associated with the density based MLD definitions (MLD(σ_T) and MLD(σ_C)), the Aegean Sea tends to be positive while it is negative in the Mediterranean Sea (Fig. 9a,b).

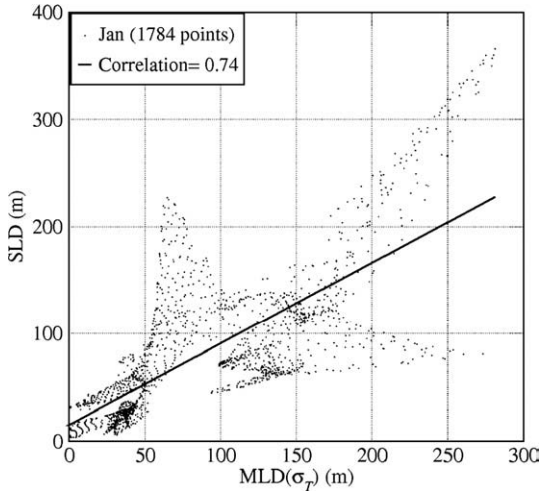

Fig. 7. Scatter diagram of SLD versus MLD(σ_T) from the January gridded field. The solid line represents the linear fit with a correlation of 0.74.

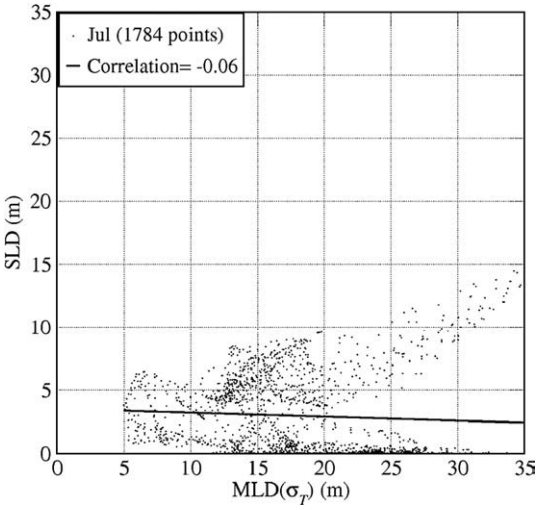

Fig. 8. Scatter diagram of SLD versus MLD(σ_T) from the July gridded field. The solid line represents the linear fit with a correlation of −0.06.

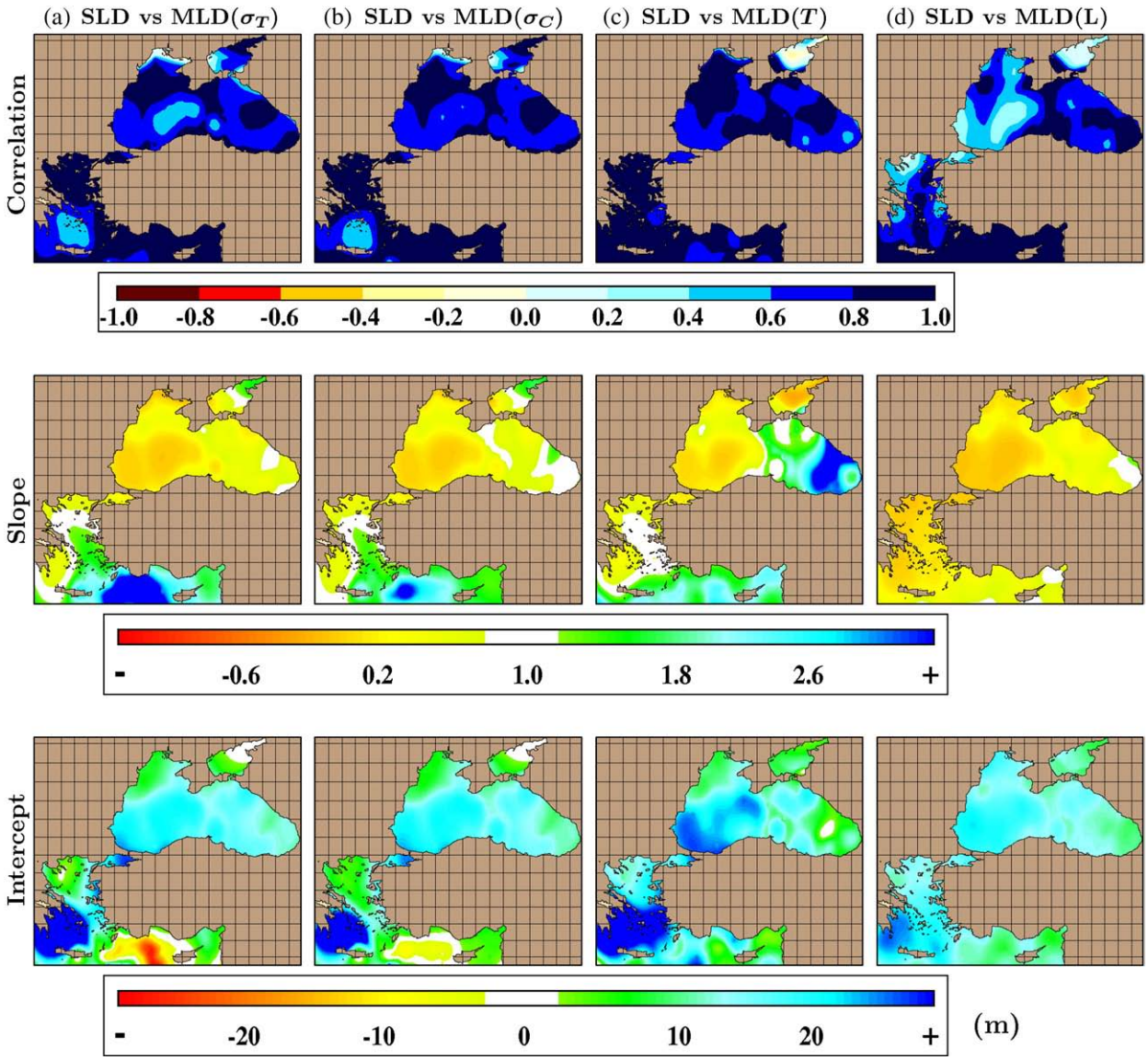

Fig. 9. Spatial variation of correlation coefficient between SLD and for each one of MLDs based on various definitions calculated over the seasonal cycle. Similarly, intercept and slope values of the least squares line are computed over the seasonal cycles as further described in the text.

Positive (negative) indicates that SLD is deeper (shallower) than MLD. For the *T*-only MLD definitions (MLD(T) and MLD(L)), the northern part of the Aegean Sea has a more positive intercept and the Mediterranean Sea is now positive (Fig. 9c,d).

7. Summary and conclusions

This paper examines the evolution over the annual cycle of the SLD relative to the MLD for the Aegean, Marmara, Black, and Azov Seas. With historical quality-controlled ocean *T* and *S* profiles, a monthly SLD climatology is constructed on a regular 025° × 0.25° grid using the kriging methodology. A four step pre-processing procedure designed to reduce noise and the effects of sampling irregularities is applied prior to forming the climatology. Monthly SLD fields are then compared relative to the much more widely studied MLD as computed using four methods from the recent scientific literature.

Very deep SLD occurs in the Aegean and Black Seas for the months of January, February, and March. This is due to the tendency of these regions to have cooler, fresher water above warmer, saltier water. When the near surface water becomes cooler than the deep water below the permanent pycnocline, the SLD drops to the bottom where sound speed is largest. When this occurs, the MLD remains at the seasonal pycnocline. This is independent of the methods used to estimate MLD, though the MLD(L) is generally shallower than MLD (σ_T) and MLD(σ_C) and has a larger bias. For the rest of the year, SLD is considerably shallower and closer to the MLD. During the spring when new stratification occurs in the Aegean Sea, SLD and MLD(L) represent the recent and shallow stratification while the MLD(σ_T), MLD(σ_C), and MLD(T) remain deeper. Long range upper ocean acoustic communication would have more favorable conditions in the months of January, February, and March in the Aegean and Black Seas.

A linear statistical relationship is established based on statistically significant correlation values between SLD and MLD. These relationships are useful for (at least) two practical purposes: (1) to determine the SLD from *T*-only profiles with the use of MLD(T) and/or MLD(L) and the linear relationship and (2) when an observation profile is deep enough to estimate the MLD but potentially not deep enough to estimate SLD. Based on computation of the error (c in Eq. (2)) a perfect linear relationship (i.e. correlation is ± 1) results in very small errors (typically <5 m). In regions where correlations are relatively lower

(e.g. 0.4–0.6), errors become larger as expected. In the regions of the Sea of Azov and mid-western Black Sea, SLD and MLD have smaller magnitudes (Fig. 5a) resulting in smaller errors, within 8 m, for all seasons except summer.

During the winter when SLD is very deep, MLD(L) has the largest bias because it tends to be a shallower MLD estimate. During the rest of the year MLD(L) is closer to SLD, but the correlation coefficient is still smaller than that for the other MLD methods. For this reason, MLD (T) may be the best predictor of SLD, when S is unavailable, using the regression analysis presented in this paper.

Acknowledgments

This work is a contribution to the Improved Synthetic Ocean Profiles project supported by the Office of Naval Research (program element 602345N). The authors thank the three anonymous reviewers for their helpful suggestions and comments. This paper is contribution NRL/JA/7320/07/8045 and has been approved for public release.

Appendix A

Four steps are applied to the SLD and MLD data before kriging interpolation is performed. These steps are designed to reduce noise and even out the relative weight of the observations.

A.1. Step 1. Z-score clipping

To minimize errors, we remove SLD and MLD outliers statistically. A common approach is to remove data values that exist outside of a standard deviation range. The problem with this method is that the standard deviation computation itself is contaminated by the outliers. To correct this problem we use in place of the standard deviation and mean the corresponding biweight estimate for the variance (scale) and mean (location), respectively (Lanzante, 1996). The biweight methodology is a robust statistical measure that accounts for non-normal distributions of data as a result of gross errors or outliers. All computation of the mean and standard deviation are therefore replaced with the biweight mean and standard deviation estimates. The removal of outlier data is then achieved using the Z-score statistic described by Lanzante (1996) and adopted by others (Zou and Zeng, 2006; Carrier et al., 2007).

The Z-score is a normalization of the data using the biweight mean and standard deviation. For a sample of n observations ($x_i, i = 1,2,3,\cdots n$) the Z-score is given by

$$Z_i = \frac{x_i - \bar{x}_{\mathrm{bi}}}{\sigma_{bi}},$$

where $\bar{x}_{\mathrm{bi}}$ is the biweight mean and σ_{bi} is the biweight standard deviation. Data are removed where the Z-score is greater than 4, indicating a deviation of 4 biweight standard deviations from the biweight mean.

A.2. Step 2. Super-observation

Climatological super-observations represent the median value and location of a data cluster from all years for a given month that are within a 1/12° circle. A set of super-observations are computed by iterating through all the original observations and replacing them with super-observations. This is done as follows:

The procedure is an iterative process for each observation ($i = 1,2,3,\ldots n$). For the ith observation, all other observations within a 1/12° circle are collected, and the median value and median location of these observations (including the ith observation) are computed. The ith observation and all other observation within the 1/12° circle are then removed and replaced with the computed median value and location. The discarded observations are not available for the rest of the process. If there are no other observations within a 1/12° circle, the ith observation is kept as is. After one pass through the observations, a new set of super-observations exists. Because the median locations of the 1/12° circles shift relative to the location of the ith observation location, some of the new super-observations are closer together than 1/12°. For this reason, additional iterative passes are conducted until no further data reductions are achieved. This occurs in 3 or 4 passes with 50% to 70% reduction in observations, with 90% of the data reduction occurring in the first pass.

A.3. Step 3. Median filter

The median filter (Tukey, 1977) is widely used in image processing for its salt and pepper noise reduction and edge preserving qualities (Maragos and Schafer, 1987). A constant time application (Perreault and Hebert, 2007) is adopted here but for irregular data. Our median filter iterates through each (super) observation, replacing its value with the median of the surrounding nearest seven observations. The location of the observation is not altered. Seven observations were chosen because for a normal distribution, sampling theory margin of error is

$$E = z_{\alpha/2}\frac{\sigma}{\sqrt{n}},$$

where $z_{\alpha/2}$ is the value for the $\alpha/2$ percent area in the right tail of the normal distribution, σ is the standard deviation, and n is the number of observations. This is a two-sided hypothesis test such that α is the percent probability that the errors are less than E. Only 7 data points are needed to achieve a 95% confidence for a margin of error that is equal to 0.75σ:

$$n = \left[\frac{z_{\alpha/2}\sigma}{E}\right]^2 = \left[\frac{z_{0.025}}{0.75}\right]^2 \approx 7$$

Since multiple applications of the median filter are recommended (Gallagher and Wise, 1981), the median filter is applied three times. Further changes are generally small for additional applications.

A.4. Step 4: Smoothing

While the median filter removes salt and pepper noise and preserves edges, it does not smooth. In order to smooth the data, a mean filter is applied to 1/2° regions around each observation. Applied in the same way as the median filter, three applications reduce noise while smoothing the horizontal gradients.

References

Beşiktepe, S.T., Sur, H.I., Özsoy, E., Latif, M.A., Oğuz, T., Ünlüata, Ü., 1994. The circulation and hydrography of the Marmara Sea. Prog. Oceanogr. 34, 285–334.

Boyer, T.P., Antonov, J.I., Garcia, H.E., Johnson, D.R., Locarnini, R.A., Mishonov, A.V., Pitcher, M.T., Baranova, O.K., Smolyar, I.V., 2006. World Ocean Database 2005. In: Levitus, S. (Ed.), NOAA Atlas NESDIS 60. U.S. Government Printing Office, Washington, D.C./USA. 190 pp.

Carrier, M., Zou, X., Lapenta, W.M., 2007. Identifying cloud-uncontaminated AIRS spectra from cloudy FOV based on cloud-top pressure and weighting functions. Mon. Weather Rev. 135, 2278–2294.

Chen, D., Busalacchi, A.J., Rothstein, L.M., 1994. The roles of vertical mixing, solar-radiation, and wind stress in a model simulation of the sea-surface temperature seasonal cycle in the tropical Pacific Ocean. J. Geophys. Res. 99, 20,345–20,359.

Cressie, N.A.C., 1991. Statistics for Spatial Data. J. Wiley, New York, NY. 900 pp.

Debolskaya, E.I., Yakushav, E.V., Kuznetsoz, I.S., 2008. Analysis of the hydrophysical structure of the Sea of Azov in the period of the bottom anoxia development. J. Mar. Syst. 70, 300–307.

Diggle, P.J., Ribeiro Jr., P.J., 2007. Model-Based Geostatistics. Springer Series in Statistics, New York, NY. 230 pp.

Etter, P.C., 2003. Underwater Acoustic Modeling and Simulation, 3rd edition. Spon Press, London/England. 424 pp.

Gallagher, N.C., Wise, G.L., 1981. A theoretical analysis of the properties of median filters. IEEE Trans. Acoust., Speech, Signal Processing ASSP-29, pp. 1136–1141.
Gould, J., Roemmich, D., Wijffels, S., Freeland, H., Ignaszewsky, M., Jianping, X., Pouliquen, S., Desaubies, Y., Send, U., Radhakrishnan, K., Takeuchi, K., Kim, K., Danchenkiv, M., Sutton, P., King, B., Owens, B., Riser, S., 2004. ARGO profiling floats bring new era of in situ ocean observation. EOS 85 (179), 190–191.
Helber, R.W., Barron, C.N., Carnes, M.R., Zingarelli, R.A., 2008. Evaluating the sonic layer depth relative to the mixed layer depth. J. Geophys. Res. 113, C07033. doi:10.1029/2007JC004595.
Kantha, L.H., Clayson, C.A., 2000. Small Scale Processes in Geophysical Fluid Flows. Academic Press, San Diego, CA. 888 pp.
Kara, A.B., Rochford, P.A., Hurlburt, H.E., 2000a. Mixed layer depth variability and barrier layer formation over the North Pacific Ocean. J. Geophys. Res. 105, 16,783–16,801.
Kara, A.B., Rochford, P.A., Hurlburt, H.E., 2000b. An optimal definition for ocean mixed layer depth. J. Geophys. Res. 105, 16,803–16,821.
Kara, A.B., Helber, R.W., Boyer, T.P., Elsner, J.B., 2009. Mixed layer depth in the Aegean, Marmara, Black and Azov Seas: Part I: general features. J. Mar. Syst. 78, S169–S180.
Kerman, B.R., 1993. Natural Physical Sources of Underwater Sound: Sea Surface Sound. Kluwer Academic Publishers, Boston. 750 pp.
Kourafalou, V.H., Barbopoulos, K., 2003. High resolution simulations on the North Aegean Sea seasonal circulation. Ann. Geophys. 21, 251–265.
Kunz, E.L., Gauss, R.E., 2000. Bottom Backscattering Measured off the Coast of Oregon During the Littoral Warfare Advanced Development 99-3 Experiment. Naval Research Laboratory. NRL/MR/7140-00-8453, 30 pp.
Lanzante, J.R., 1996. Resistant, robust and non-parametric techniques for the analysis of climate data: theory and examples, including applications to historical radiosonde station data. Int. J. Climatol. 16, 1197–1226.
Lorbacher, K., Dommenget, D., Niiler, P.P., Kohl, A., 2006. Ocean mixed layer depth: a subsurface proxy of ocean-atmosphere variability. J. Geophys. Res. 111, C07010. doi:10.1029/2003JC002157.
Mackenzie, K.V., 1981. Nine-term equation for sound speed in the ocean. J. Acoust. Soc. Am. 70, 807–812.
Maragos, P., Schafer, R.W., 1987. Morphological filters — Part II: their relations to median, order-statistic, and stack filters. IEEE Trans. Acoust. Speech Signal Process. 35, 1170–1184.
Matishov, G., Matishov, D., Gargopa, Y., Dashkevich, L., Berdnikov, S., Baranova, O., Smolyar, I., 2006. Climate Atlas of the Sea of Azov 2006. In: Matishov, G., Levitus, S. (Eds.), NOAA Atlas NESDIS 59. U.S. Government Printing Office, Washington, D.C., USA. CD-ROM, 103 pp.
Olson, D.B., Kourafalou, V.H., Johns, W.E., Samuels, G., Veneziani, M., 2007. Aegean surface circulation from a satellite-tracked drifter array. J. Phys. Oceanogr. 37, 1898–1917.
Özsoy, E., Ünlüata, Ü., 1998. In: Robinson, A., Brink, K. (Eds.), The Black Sea. The Sea, vol. 11. John Wiley, Hoboken, NJ, pp. 889–914.
Perreault, S., Hebert, P., 2007. Median filtering in constant time. IEEE Trans. Image Process. 16, 2389–2394.
Poulain, P.-M., Barbanti, R., Motyzhev, S., Zatsepin, A., 2005. Statistical description of the Black Sea near-surface circulation using drifters in 1999–2003. Deep-Sea Res. I 52, 2250–2274.
Siderius, M., Porter, M.B., Hursky, P., McDonald, V., 2007. Effects of ocean thermocline variability on noncoherent underwater acoustic communications. J. Acoust. Soc. Am. 121, 1895–1908.
Siegel, D.A., Doney, S.C., Yoder, J.A., 2002. The North Atlantic spring phytoplankton bloom and Sverdrup's critical depth hypothesis. Science 296, 730–733.
Sutton, P.J., Worcester, P.F., Masters, G., Cornuelle, B.D., Lynch, J.F., 1993. Ocean mixed layers and acoustic pulse-propagation in the Greenland Sea. J. Acoust. Soc. Am. 94, 1517–1526.
Teague, W.J., Carron, M.J., Hogan, P.J., 1990. A comparison between the generalized digital environmental model and Levitus climatologies. J. Geophys. Res. 95, 7167–7183.
Tukey, J., 1977. Exploratory Data Analysis. Addison-Wesley, Menlo Park, CA. 688 pp.
Urick, R.J., 1983. Principles of Underwater Sound, 3rd edition. McGraw-Hill, Los Altos, CA. 423 pp.
Wilks, D.S., 1995. Statistical Methods in the Atmospheric Sciences. Academic Press, San Diego. 467 pp.
Zou, X., Zeng, Z., 2006. A quality control procedure for GPS radio occulation data. J. Geophys. Res. 111, D02112. doi:10.1029/2005JD005846.